Journal of Hydrology 526 (2015) 55–67

Contents lists available at ScienceDirect

Journal of Hydrology

journal homepage: www.elsevier.com/locate/jhydrol

Comparative analysis of drought based on precipitation and soil moisture indices in Haihe basin of North China during the period of 1960–2010

Yue Qin, Dawen Yang *, Huimin Lei, Kai Xu, Xiangyu Xu

State Key Laboratory of Hydroscience and Engineering, Department of Hydraulic Engineering, Tsinghua University, Beijing 100084, China

ARTICLE INFO

Article history:
Available online 5 October 2014

Keywords:
Drought analysis
Standardized Precipitation Index (SPI)
Soil Moisture Drought Severity (SMDS)
Community Land Model
Haihe basin

SUMMARY

Drought severity not only depends on weather anomaly, but is also related to terrestrial hydrological condition to a large extent. In this study, we analyzed droughts using indices based on precipitation and soil moisture during the period of 1960–2010 in Haihe basin, which is a typical drought-prone region in North China. The Soil Moisture Drought Severity (SMDS) and Standardized Precipitation Index (SPI) are used to evaluate drought severity. SMDS is calculated based on the monthly soil moisture of upper 50 cm from the simulation by Community Land Model (CLM 4.0) and SPI is calculated based on gridded precipitation at 0.05° resolution (5 km × 5 km approximately), which is spatially interpolated from observations. During the last 51 years, 36 severe drought events (affecting areas greater than 20,000 km^2 and durations longer than 3 months) have been identified based on SMDS, and 41 drought events identified based on SPI. Results derived from SMDS indicate that there is a significant increasing trend in the drought affected area, and that the drought event occurred in 1999 has the largest affected area. Compared with the drought events derived from SMDS, the events derived from SPI have shorter durations but larger affected areas on average. Although the mean NDVI of the whole basin has been increasing since the 1980s, the two declining periods of 1992–1994 and 1999–2003 show fairly good agreement with the drought events identified in the same periods. The Anomaly of Normalized Difference Vegetation Index (A-NDVI) is introduced as NDVI anomaly from its trend line, thus the negative value of A-NDVI can reflect the drought impact on vegetation reasonably. Result indicates that both the SMDS and SPI are significantly correlated with A-NDVI, and correlation between annual SMDS and A-NDVI is higher than that of SPI.

1. Introduction

In the past few decades, in the context of climate change and the fast development of socio-economic conditions, drought has become one of the most serious natural disasters that has caused significant damages to the human society (Federal Emergency Management Agency, 1995; National Climatic Data Center, 2003; Bryant, 2005). According to statistics, China's drought-induced loss of grain production exceeded 26 billion kilogram per year, which was almost the annual food demand of 60 million people (Li et al., 2010). Since the 1990s, drought and desertification had an increasing trend in North China and caused annual economic losses in excess of $12 billion (Fu and An, 2002). Wang et al. (2011) reported that drought had an increasing trend in the past 50 years over the mainland of China, and Zhai et al. (2010b) pointed out that drought frequency has increased in major basins in North China. For quantitative disaster assessment, drought analysis is an increasingly important topic in recent hydrological research.

However, due to the complex nature of drought, most of drought definitions are based on the context of applications (Andreadis et al., 2005). Two widely recognized definitions are: (1) levels of precipitations lower than normal and durative shortage of water resources (World Meteorological Organization, WMO, 1986, 2012), which is usually defined as meteorological drought; (2) the soil water content below annual average value accompanied with reduction of grain yield (Food and Agricultural Organization of United Nations, FAO, 2002), which is usually defined as agricultural drought. In this study, we focused on the meteorological and agricultural droughts in the past 5 decades of Haihe basin in North China.

Meteorological drought is linked to the water shortage caused by abnormal meteorological conditions, such as the lack of rainfall and high temperature. Therefore, the index of meteorological

* Corresponding author.
E-mail address: yangdw@mail.tsinghua.edu.cn (D. Yang).

http://dx.doi.org/10.1016/j.jhydrol.2014.09.068
0022-1694/

drought mainly considers parameters like precipitation, temperature, humidity, and so on. The Standardized Precipitation Index (SPI) (McKee et al., 1993, 1995) is a commonly used meteorological drought index in many studies. It is comparable across different climatic regions (Guttman, 1998), and has been widely used in drought assessment (Zhang et al., 2009; Zhai et al., 2010a; Fischer et al., 2011; Zhao et al., 2012; Hao and AghaKouchak, 2013; Gocic and Trajkovic, 2013).

Agricultural drought is usually defined based on the deficit of soil water, which has a direct impact on the crop growth. Agricultural drought is influenced by multiple factors, such as soil moisture, crop type, and irrigation. Thus, the drought intensity is often characterized by the soil moisture or the crop/vegetation state. For instance, the Crop Moisture Index (CMI) (Palmer, 1968) and Water Deficit Index (WDI) (Moran et al., 1994) have been introduced in previous studies. Soil water storage is a key part in the terrestrial hydrologic cycle, and it also connects the groundwater with vegetation. In this study, we described the agricultural drought based on the empirical probability distribution of soil moisture, which is defined as the Soil Moisture Drought Severity (SMDS). Soil moisture and the related parameters have been widely used to describe drought impacts on the vegetation, cropland or groundwater storage (Andreadis et al., 2005; Wang et al., 2011; Long et al., 2013; Thomas et al., 2014).

When the drought breaks out in a certain region, what really should be concerned about is the available water on the land surface. Thereby, the evaluation of droughts should consider both the water supply by precipitation and the water dissipation on land surface. The water dissipation is mainly related to the canopy interception, evapotranspiration (ET), and soil water storage. All these processes can be simulated by physically based hydrological models or land surface models, such as the Variable Infiltration Capacity (VIC) model and Community Land Model (CLM). These models are commonly used to analyze the spatial and temporal patterns of major droughts by their spatial and temporal continuous simulations, and have been widely applied for drought assessment during the last several decades (Andreadis et al., 2005; Sheffield and Wood, 2007; Sheffield et al., 2009; Wang et al., 2011). Most such studies focused on the trend of large-scale droughts based on a single index, but lacked the detailed analysis of typical drought-prone regions and inter-comparison of different indices.

In this study, we selected Haihe basin in North China as the study domain. The main objectives are: (1) to characterize major drought events spatially and temporally in this region; (2) to understand the changes of drought events during the last 51 years; (3) to compare the applicability of the soil moisture drought index with precipitation drought index in the perspective of terrestrial ecosystem, especially the vegetation growth.

In the sections that follow, the hydrological and meteorological features of the study area are first presented followed by the data and the land surface model (CLM) used, and the methods used to analyze drought. In the section on results, the drought temporal trend and spatial pattern in the study area are given first followed by the details of major drought events. Finally, a comparison between the precipitation-based drought index and the soil-moisture-based index is given.

2. Study area and data

2.1. Haihe basin and the historical droughts

Haihe basin is one of the largest basins in North China, and contains several large cities (e.g., Beijing and Tianjin) with a total population of 137 million. Its area measures around 318,800 km^2, of which mountainous area (elevation above 100 m; Lei et al., 2014) accounts for about 60% (see Fig. 1). The plain area of the basin is

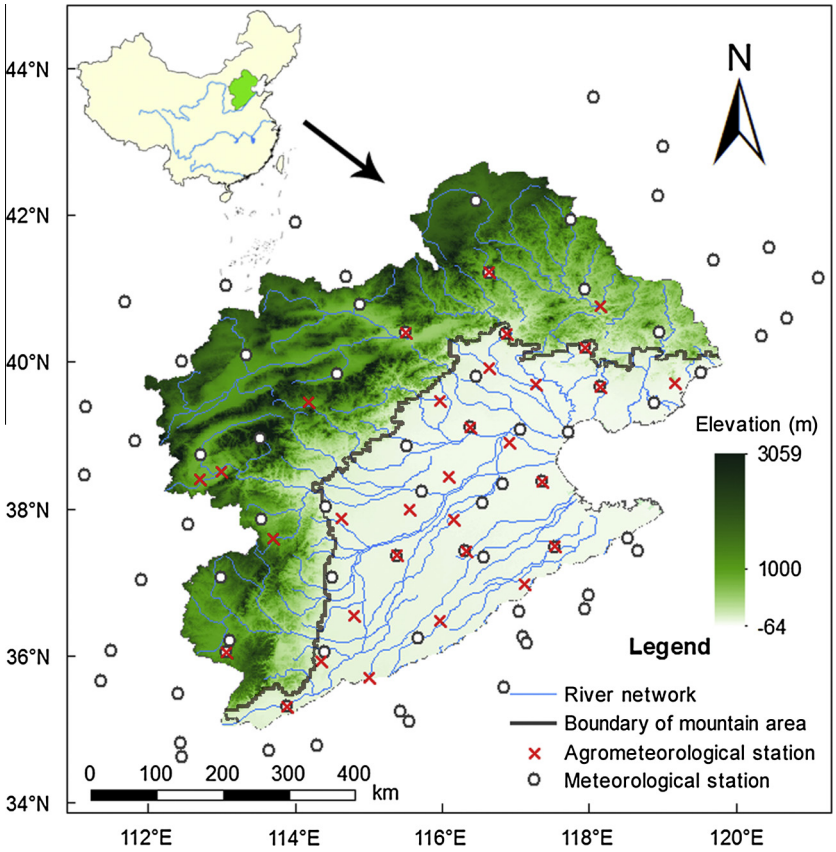

Fig. 1. Topographic map of Haihe basin and location of observation stations (circle represents meteorological station; cross represents agrometeorological station).

one of the major grain producing areas in China, which contributes about 9.4% of the annual grain yield in the country (Haihe River Commission, 2012). Haihe basin belongs to the temperate continental monsoon climate. Its mean annual precipitation is approximately 530 mm with highly seasonal and interannual variability. In winter (December–February), controlled by Siberian high pressure, it is often dry with less precipitation while in spring (March–May), temperature rises rapidly and the actual evaporation is high because of the strong wind. Nearly 70% of annual precipitation is concentrated from June to September. China Meteorological Administration (CMA, 2007) analyzed the drought frequency in China from 1961 to 2006, and the results showed that the North China Plain is one of the regions suffering frequent droughts.

From the literature survey, the drought characteristics in Haihe basin can be summarized as: (1) frequent seasonal water deficit in the basin attributed to meteorological and/or geographic reasons (Bao et al., 2012; Xu et al., 2014); (2) droughts in spring had the largest impact on agricultural production in plain area (Haihe River Commission, 2004a); (3) several prolonged drought events occurred in history (Lu et al., 2011), which have been verified by tree-ring cellulose in the North China Plain (Li et al., 2011b) and by the ancient records on oracle bones in the 11th century B.C. (Haihe River Commission, 2004b).

2.2. Data preparation

In this study, the forcing data for running version 4.0 of the Community Land Model (i.e., CLM 4.0) includes the historical climatic data and the land surface parameters. The historical climatic data were obtained from 73 meteorological stations in the basin and its surrounding area as shown in Fig. 1, which were originally provided by the National Meteorological Information Center (NMIC) of CMA and downloaded from China Meteorological Data Sharing System (CMDSS) (http://cdc.cma.gov.cn). The observed meteorological data included daily precipitation, air temperature (maximum, minimum, and average), daily sunshine duration, average wind speed and relative humidity. This dataset is available from January 1960 to December 2010, and the daily data were downscaled to 3-hourly data by the empirical methods proposed by Lei et al. (2013). Gridded data of $0.05^\circ \times 0.05^\circ$ resolution were interpolated using an angular distance weighting method (Yang et al., 2004) and used in the CLM 4.0.

Fig. 2a illustrates the spatial distribution of annual precipitation in the study domain. The hilly region in the north of basin has relatively lower mean precipitation than the southern plain, and rainfall depth of most areas is above 400 mm. Fig. 2b shows that the annual precipitation has a significant decreasing trend (−15.7 mm/decade) in the past 51 years. There are clearly two dry spells in 1980–1984 and 1999–2002.

Regarding the land surface parameters, in this study, the soil texture data were obtained from Shangguan et al. (2012) which contained textures of surficial (0–30 cm) and underlying (30–100 cm) soil layers. Land use/cover data in 1985 were obtained from the Environmental & Ecological Science Data Center for West China (EESD) (http://westdc.westgis.ac.cn) (Liu et al., 2005) and were converted into land cover types used in CLM 4.0.

The Normalized Difference Vegetation Index (NDVI) data were used directly to assess the drought impacts on the terrestrial

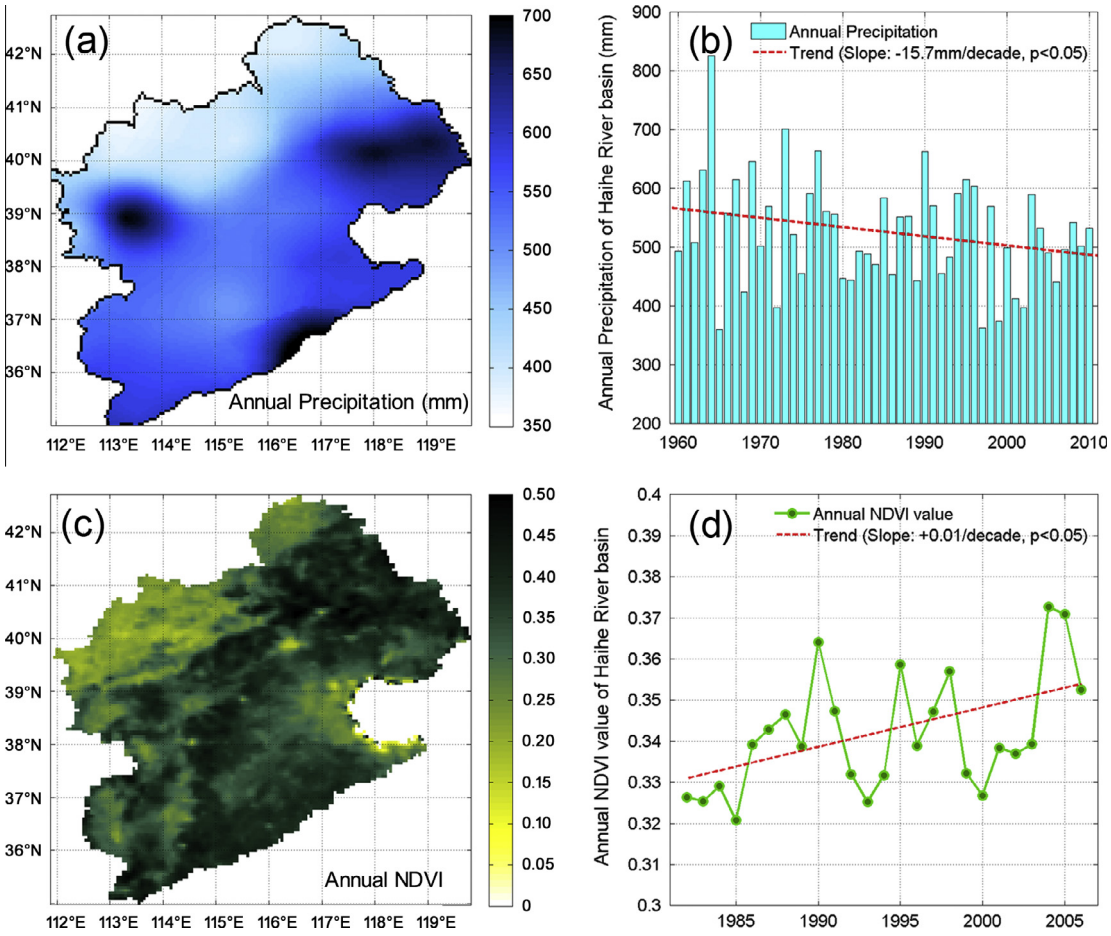

Fig. 2. (a) Distribution of annual precipitation (mm) in Haihe basin in 1960–2010; (b) interannual variation and trend of annual precipitation; (c) spatial distribution of annual mean NDVI from 1982 to 2006; (d) interannual variation and trend of annual mean NDVI.

ecosystem. This study used the GIMMS (Global Inventory Monitoring and Modeling Studies) NOAA/AVHRR NDVI datasets downloaded from EESD (Xu et al., 2014). The NDVI dataset was available monthly from 1982 to 2006 with a resolution of 8-km. Fig. 2c illustrates the distribution of mean NDVI in the basin. It shows that the northwest mountainous area has relatively lower NDVI than the plain area. The annual mean NDVI is increasing by 0.01/decade as illustrated in Fig. 2d. However, there are two periods in which the annual NDVI is lower than the average, namely 1992–1994 and 1999–2003.

In order to verify soil moisture simulated by the model, a 10-day 50-cm soil moisture dataset (CMA, 1993) at 31 China Agrometeorological Stations (note: different from the meteorological stations, see Fig. 1) in the basin was collected. This dataset is from the NMIC of CMA, and is available from January 1991 to December 2010. The CMA soil moisture data is given as the relative soil moisture that is defined as $R = \theta/\theta_f \times 100\%$ (CMA, 1993), where θ is the volumetric soil water content, and θ_f is the volumetric soil water content at field capacity. Parameter θ_f is estimated as $\theta_f = \theta_s(\psi_s/\psi_f)^{1/B}$ given the soil water parameters and $\psi_f = -33$ kPa, which are the same parameters used in the CLM 4.0. We selected the stations with few missing data and converted relative soil moisture into volumetric soil water content for validating the simulated soil moisture by CLM 4.0.

3. Methodology

3.1. Community Land Model and its simulated soil moisture

CLM 4.0 (Oleson et al., 2010; Lawrence et al., 2011) is a process-based terrestrial ecosystem model that simulates land surface processes under various climate situations. Highlights of CLM 4.0 include the integrated expression of biophysical and biogeochemical cycles as key parts in the land surface processes. Hydrologic cycle in CLM 4.0 includes the canopy interception, soil water movement, snow melt, ET process and so on. The soil water dynamics of this model focuses on infiltration, redistribution of water in vertical direction, and the sub-surface drainage. CLM 4.0 and its previous versions have been evaluated widely by flux data and soil moisture sampling (Stöckli et al., 2008; Wang and Zeng, 2011; Hou et al., 2012) and the simulations have been used in various scales studies (Li et al., 2011a; Huang et al., 2013; Shi et al., 2013).

The simulations of CLM 4.0 were run from 1960 to 2010 at 0.05° resolution (5 km × 5 km approximately) over Haihe basin, forced by the historical climatic data and the land surface parameters introduced in Section 2.2. The simulations are described in detail by Lei et al. (2014) and have been validated using available observations, such as the stream discharge, remote sensing-based ET, gross primary production (GPP), leaf area index (LAI), etc. This study used the simulation of soil moisture for drought analysis. Monthly average volumetric soil water content (cm^3/cm^3) of the top 50-cm depth (represents the root zone) for each CLM 4.0 grid cell is calculated from January 1960 to December 2010.

Based on the observed soil moisture, the simulation of CLM 4.0 was validated again in this study. Fig. 3a compares the simulated and observed soil moisture at the 31 stations. Generally, the simulation of model in Haihe basin is significantly correlated with observation (correlation coefficient $R = 0.72$) and the deviation is in an acceptable range. As illustrated in Fig. 3b, both the simulated and observed soil moistures have a consistent interannual variability, and simulated soil moisture shows a greater variability compared to the observed one. The reason for this high variability of the simulated soil moisture may be due to the reduction of soil moisture deficit especially during the drought years by agricultural irrigation, which is not considered in the CLM simulation used in this study. Therefore, this high variability of soil moisture reflects the natural hydrological condition reasonably.

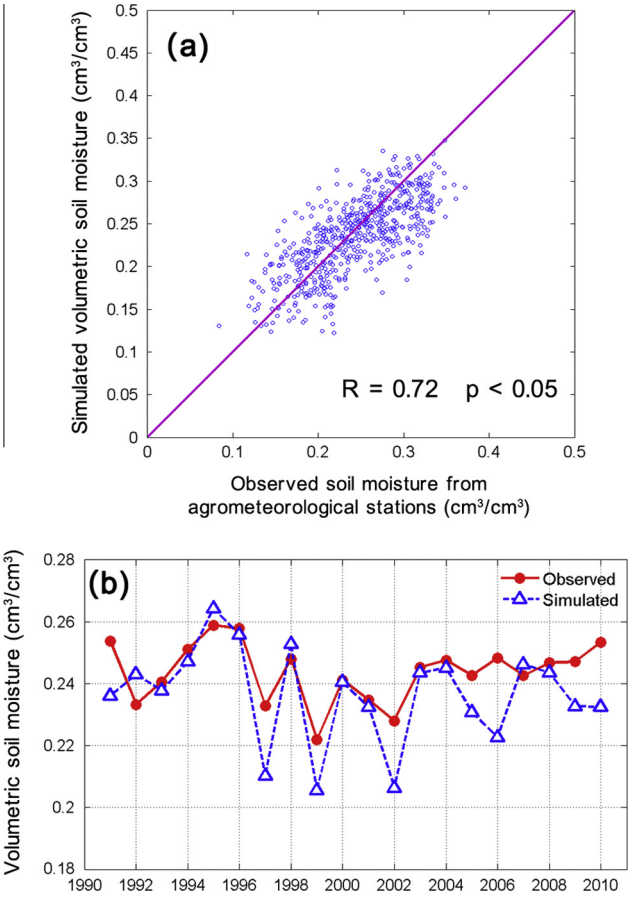

Fig. 3. (a) Comparison of CLM-simulated and observed monthly soil moisture of top 50-cm during the period of 1991–2010; (b) interannual variations of CLM-simulated and observed average soil moistures. (*Note:* the volumetric water content is converted from the relative soil moisture obtained from CMA).

3.2. Calculation of Soil Moisture Drought Severity

As drought is a relative rather than an absolute condition, a probability-based index is applied for direct drought severity evaluation across different regions. Probability distribution function of drought index can be estimated by at least 20 years of data. The most widely used probability distribution functions include gamma distribution, Pearson Type III distribution, and empirical cumulative probability distribution (McKee et al., 1993; Guttman, 1999; Andreadis et al., 2005).

Empirical cumulative probability function is applied in this study to estimate the probability (percentile) of soil moisture droughts in each month of the past 51 years for each grid cell, which is expressed as:

$$P = \frac{m}{n+1} \times 100\% \quad (1)$$

where P is the soil moisture percentile (SMP) of a specific cell in a month of a specific year in the 51-year statistics, m is the rank number of soil moisture value of the same month of the specific year in the 51-year time series in the order from low to high, and n refers to the sample size which equals 51 in this study. Thus the smaller P value (lower soil moisture) means more severe drought.

Drought severity is an integrated index of intensity and duration, and refers to the cumulative deficit of the index below a given threshold value (Yevjevich, 1967; Mishra and Singh, 2010). In this

study, we used the probability-based definition of drought severity introduced by Andreadis et al. (2005) which is expressed as:

$$S = 1 - \sum_{i=1}^{t} P_i / t \tag{2}$$

where S is the Soil Moisture Drought Severity (SMDS), P_i is the SMP in Eq. (1), t is the summed time steps with the unit of month. In particular, if time step is one month ($t = 1$), then SMDS is expressed as $S = 1 - P$. Obviously, a larger value of S refers to a greater impact of drought. Then drought severity is expressed by the index SMDS in the range of 0–1.

For regional prolonged droughts, a full-scale analysis of all the droughts is hard to achieve. This study only chose major droughts with significant impacts for analysis. The common method is to define a drought index threshold below which the breakout of drought is recognized (Dracup et al., 1980; Andreadis et al., 2005; Sheffield et al., 2009). Climate Prediction Center (CPC) of NOAA, U.S. categorizes droughts based on the SMP in Eq. (1) in the following scheme: moderate drought (11–20%), severe drought (6–10%), extreme drought (3–5%), and exceptional drought (0–2%) (U.S. Drought Monitor, 2003; Climate Prediction Center, 2005). In accordance with the CPC scheme, we defined threshold of SMP as 20%. Therefore, if the monthly SMDS of a grid cell is lower than 80%, then this cell is not identified as in a drought condition in this month.

3.3. Calculation of Standardized Precipitation Index

Precipitation is a major index for drought evaluation, and long-term observations are available in most areas. The Standardized Precipitation Index (SPI) is an ingenious index based on standardized probability to quantify precipitation deficit (WMO, 2012). The calculation procedure of SPI is based on long-term precipitation observations. The precipitation data series are firstly fitted into a proper probability distribution. The inverse normal function is then applied to the cumulative probability, and the result is the SPI (Guttman, 1998, 1999). One of the notable strengths of SPI is the normalized probability distribution (see Fig. 4), so that both the dryness and wetness can be compared across different regions.

The numerical value of SPI refers to standard deviation of measured precipitation from a given probability distribution function. Suppose x is the cumulated monthly precipitation in the time scale of research (1-month, 3-month, 6-month, 12-month, etc.) which fits a gamma probability density function $g(x)$ as follows:

$$g(x) = \frac{1}{\beta^{\alpha}\Gamma(\alpha)} x^{\alpha-1} e^{-x/\beta}, \quad x > 0 \tag{3a}$$

$$\Gamma(\alpha) = \int_0^{\infty} x^{\alpha-1} e^{-x} dx \tag{3b}$$

where x is the precipitation sum, $\Gamma(\alpha)$ is the Gamma function. In Eqs. (3a) and (3b), α and β are the shape and scale parameter respectively, which can be estimated by the maximum likelihood method (Guttman, 1999; Yuan and Zhou, 2004; Liu et al., 2012) as follows:

$$\alpha = \frac{1 + \sqrt{1 + 4A/3}}{4A}, \quad \beta = \frac{x}{\alpha} \tag{4a}$$

$$A = \ln(\bar{x}) - \frac{\sum \ln(x)}{n} \tag{4b}$$

where n is the length (months) of the time series. Then the cumulative probability of precipitation x in the given time scale is expressed as:

$$G(x) = \int_0^x g(x)dx = \frac{1}{\beta^{\alpha}\Gamma(\alpha)} \int_0^x x^{\alpha-1} e^{-x/\beta} dx \tag{5}$$

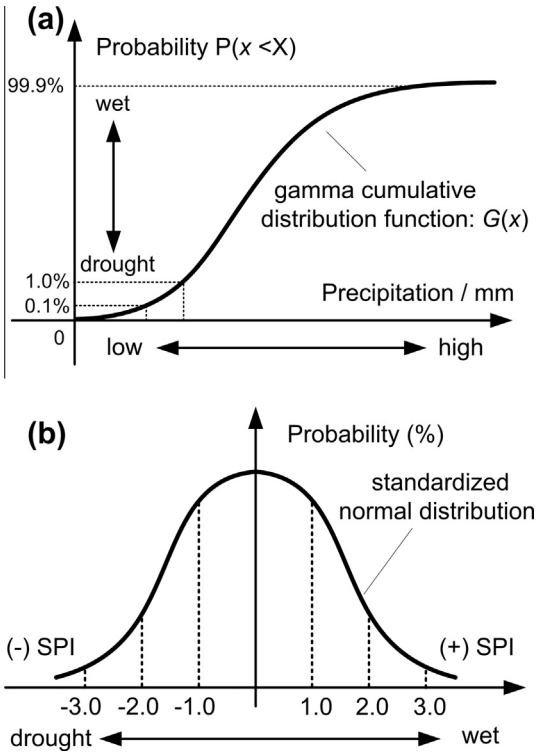

Fig. 4. Sketch of the normalized distribution applied by the Standardized Precipitation Index: (a) fitted gamma distribution for the cumulated monthly precipitation in Eqs. (5) and (6); (b) standardized normal distribution for SPI in Eq. (8). Wetness is expressed by positive SPI values while dryness by negative values.

Let $t = x/\beta$ and Eq. (5) above transforms into an incomplete Gamma function:

$$G(x) = \frac{1}{\Gamma(\alpha)} \int_0^x t^{\alpha-1} e^{-t} dt \tag{6}$$

Eq. (6) does not consider the extreme situation when the cumulated monthly precipitation $x = 0$. As a result, the equation is then modified as $H(x)$:

$$H(x) = q + (1 - q)G(x) \tag{7}$$

where q is the probability of $x = 0$, that is, the frequency of occurrence of $x = 0$ in the whole observation series. When transformed into the standardized normal distribution function, the SPI is expressed as:

$$\mathrm{SPI} = \begin{cases} -\left(t - \frac{c_0 + c_1 t + c_2 t^2}{1 + d_1 t + d_2 t^2 + d_3 t^3}\right), & t = \sqrt{\ln\left(\frac{1}{H(x)^2}\right)}, \quad 0 < H(x) \le 0.5 \\ t - \frac{c_0 + c_1 t + c_2 t^2}{1 + d_1 t + d_2 t^2 + d_3 t^3}, & t = \sqrt{\ln\left(\frac{1}{(1 - H(x))^2}\right)}, \quad 0.5 < H(x) < 1 \end{cases} \tag{8}$$

where the constants $c_0 = 2.515517$, $c_1 = 0.802853$, $c_2 = 0.010328$, $d_1 = 1.432788$, $d_2 = 0.189269$, $d_3 = 0.001308$.

The standardized distribution allows SPI to determine the rarity of a current drought event (see Table 1), and the return periods of droughts are estimated as well (Mishra and Singh, 2011; WMO, 2012). In order to compare with soil moisture drought index (SMDS), the time scale of SPI was selected as 3 month (denoted as SPI-3) as suggested by WMO (2012). In addition, the threshold of SPI was selected as −0.85, which is the 20% probability quantile of standardized normal distribution. If the monthly SPI of a grid cell is greater than −0.85, then the cell is not identified as in a drought condition. This threshold makes drought severity derived from SPI comparable with that from SMDS under the CPC scheme.

Table 1
Drought classifications based on the Standardized Precipitation Index.

Categories	SPI values	Probability (%)	Return period of drought
Mild dryness	−0.99 to 0.00	34.1	1 in 3 years
Moderate dryness	−1.49 to −1.00	9.2	1 in 10 years
Severe dryness	−1.99 to −1.50	4.4	1 in 20 years
Extreme dryness	−2.00 and less	2.3	1 in 50 years
Selected threshold in this study	−0.85 and less	20.0	1 in 5 years

3.4. Anomaly of Normalized Difference Vegetation Index

As shown in Fig. 2, the annual NDVI has a significant increasing trend which may be induced by the expansion of agriculture irrigation in the plain areas and the soil–water conservation practice in mountain areas. In order to describe the drought impacts on terrestrial ecosystems, this study introduces the Anomaly of Normalized Difference Vegetation Index (A-NDVI). Meteorologically, the term "anomaly" means deviation between the observed value and the normal level, and the long-term mean is usually used as the normal level. In this study, we define the normal level as that represented by the linear trend line of NDVI in the study period. Thus, A-NDVI is defined as:

$$A\text{-}NDVI(x) = NDVI(x) - T\text{-}NDVI(x) \quad (9)$$

where $NDVI(x)$ is the annual average NDVI of the basin in the year x, and $T\text{-}NDVI(x)$ is the NDVI value obtained from the trend line of NDVI corresponding to year x. This study uses the linearly fitted trend as illustrated in Fig. 2d. Positive values of *A-NDVI* imply that the vegetation grows better than the normal level, and vice versa.

Compared with the NDVI anomaly used in previous studies (Anyamba et al., 2001), the main advantage of *A-NDVI* used in this study is that it removes the trend component induced by the non-stationary changes. The NDVI anomaly from the trend line reflects the drought impact better, rather than the NDVI anomaly from the long-term average line does.

4. Results

4.1. Drought trend in the past 51 years

Based on the given thresholds (SMDS > 0.80, SPI-3 < −0.85) for the monthly drought indices, grid cells in drought condition are identified, and the drought affected areas are calculated. Seasonal and annual averages are calculated from drought affected areas in each month. The seasonal average area is the mean value of 3-month drought affected areas: winter from December to February, spring from March to May, summer from June to August, and autumn from September to November. Fig. 5 illustrates the inter-annual variations of drought affected areas. Mann–Kendall trend test (Mann, 1945; Kendall, 1975) is used to detect the trends of drought affected area in the past 51 years.

The annual drought affected area has an increasing trend with significance level 0.05 based on the SMDS index. In particular, the drought affected area increased dramatically after 1980. This increasing trend is consistent with the results given by some larger-scale studies in China (Sheffield and Wood, 2008; Wang et al., 2011). Specifically, the drought that occurred in 1965 is the most extensive in the 1960s, and affected almost 30% of the whole basin area. In the 1970s, drought affected area percentiles are uniformly below 20%. The post-1980 years with affected area over 30% are 1980, 1981, 1984, 1992, 1997, 1999, 2000, 2002, 2006 and 2009. Specifically, the 1999 drought stands out with the largest area in the past 51 years.

The drought affected areas in each season are also shown in Fig. 5. Based on SMDS, the drought affected areas in winter and spring have a significant increasing trend with significance level 0.05. Comparing the annual and seasonal drought affected areas, it is apparent that most of the large-scale droughts occurred in winter, spring and summer, such as the droughts that occurred in 1981, 1992, 1999–2000 and 2006.

Fig. 5 also compares the drought affected area based on SPI with that of SMDS. In general, both of the indices showed similar results. For instance, the largest drought affected area is in the early 2000s, and after 1980 the major drought years (in terms of drought affected area) are 1984, 1999, and 2006. However, an apparent difference is that the trend of the SPI-based drought affected area is non-significant. In addition, the 1960s drought period derived from SPI stands out with a larger affected area than that of SMDS, particularly in 1965 and 1968. One possible explanation is the influence of the groundwater, because the groundwater level in the North China Plain was much shallower in the 1960s than after the 1980s. Thereby the deficit in precipitation did not lead to a large-scale soil moisture drought in the 1960s.

4.2. Spatial patterns of the droughts

Spatial distributions of several typical droughts derived from SMDS and SPI are illustrated in Figs. 6 and 7 for three typical droughts that occurred in 1965, 1981 and 1999. The darker color in the maps refers to relatively higher drought intensity. As illustrated in Fig. 6, drought in August 1965 was mainly concentrated in the western part of the basin whereas drought in April 1981 occurred in the northern part and the southern part of the basin. The drought in August 1999 was the most spatial extensive one, and concentrated in the southeastern part of the basin.

Fig. 6 also shows the agricultural drought affected area (using SMDS) both in plains and in mountains. It can be seen that drought in mountainous area (northern and western part of basin) has shown a gradually decreasing trend since the 1980s, with the largest affected area in 1981 covering more than 60% of whole mountainous area. On the contrary, drought in the plain area (southern and eastern part) presents an increasing trend in the recent 30 years, and the largest area corresponded to the two droughts in 1999–2000 and 2002, covering nearly 80% of the whole plain area. During the period of 1990–2005, drought affected larger areas in plain than in mountain, particularly for the droughts in 1998, 2000 and 2002.

Drought spatial features derived from SPI are shown in Fig. 7. They generally show good agreement with those derived from SMDS. However, the most notable differences is that droughts derived from SPI in the 1960s covered a comparatively larger area (covering nearly 50% of basin) than those derived from SMDS. Besides, the drought in April 1981 covered a smaller area (30% of basin) by SPI than that by SMDS and only affected the southern part of the basin, while the 1972 drought affected area increases from 20% by SMDS to about 40% by SPI.

4.3. Characteristics of severe drought events

For further analysis, several severe drought events are selected in the following part with long durations and large affected areas. Similar to the severity–area–duration (SAD) analysis proposed by Andreadis et al. (2005), we analyzed the changes of drought events in space and time during the past 51 years.

For data preprocessing, the monthly drought severity is first smoothed by a 3×3 moving median filter. The smoothing process is used to filter the abnormal value, as the prominent spatial characteristic of a drought event is the contiguity of its extent (Andreadis et al., 2005). Then, based on clustering algorithm, major drought events are identified by their temporal connectivity from

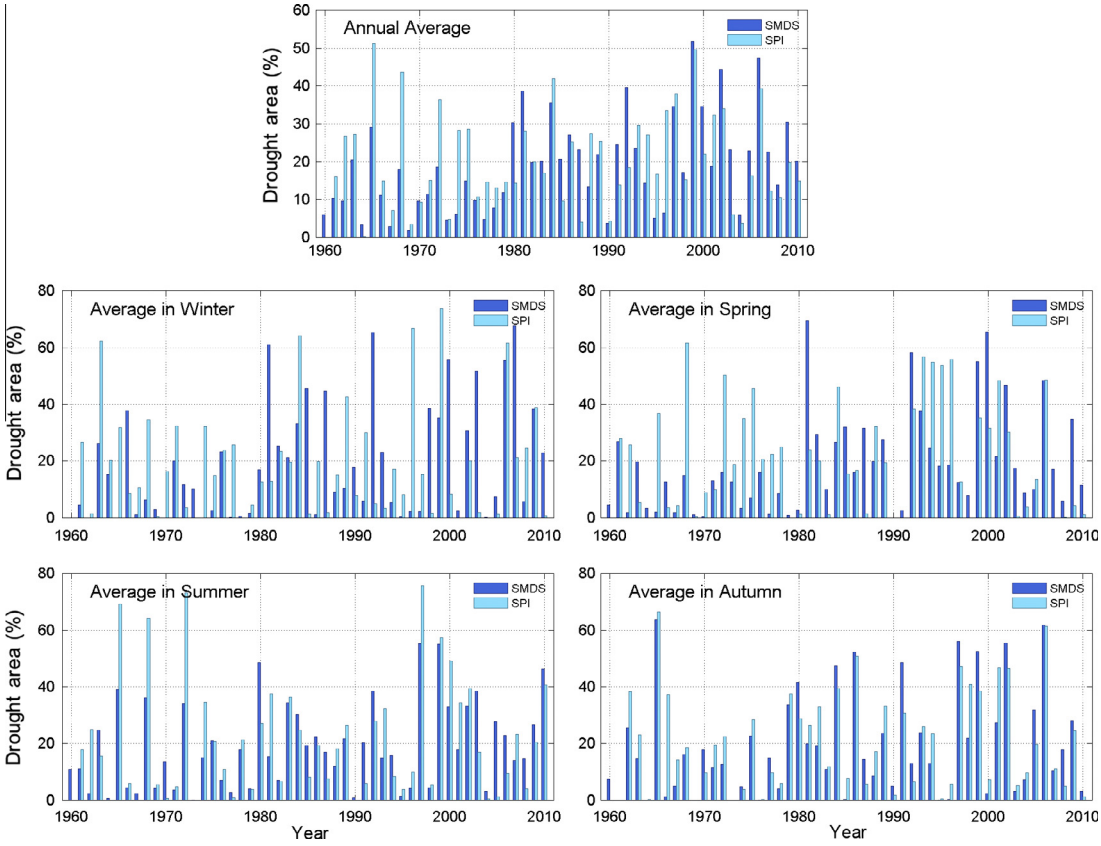

Fig. 5. Drought affected areas during 1960–2010 using SMDS and SPI. The drought affected area is calculated monthly and averaged in the annual scale, in winter (December–February), in spring (March–May), in summer (June–August) and in autumn (September–November).

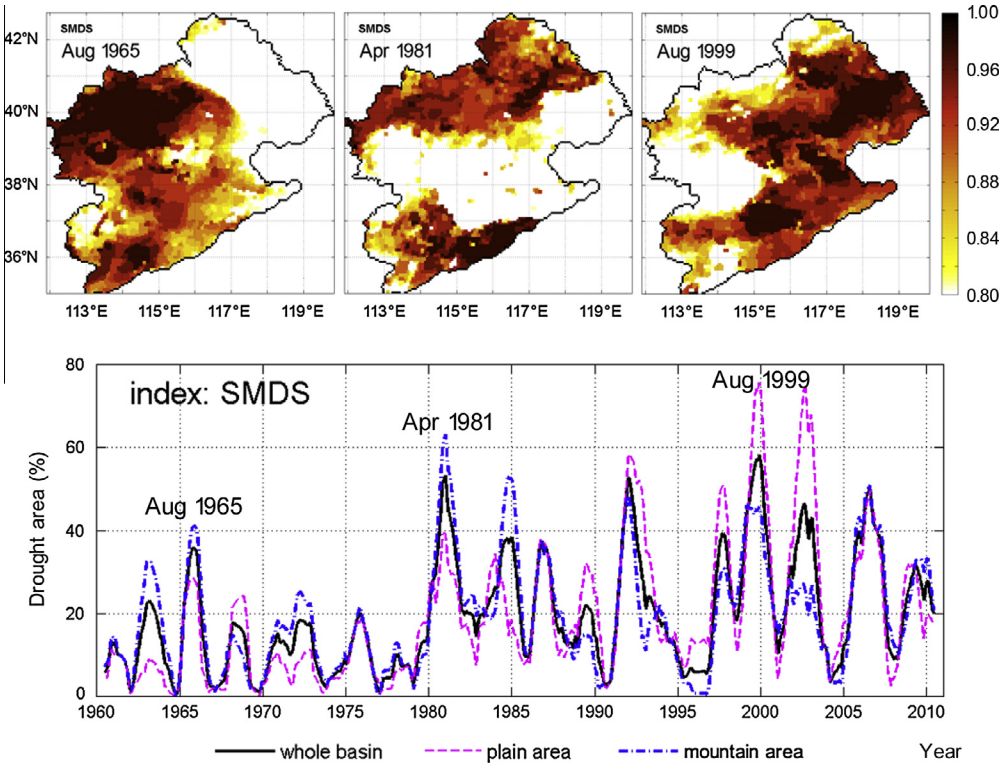

Fig. 6. Spatial patterns of three major droughts and the drought affected areas from 1960 to 2010 derived from the SMDS. The color bar in upper three maps refers to the drought severity given as SMDS value. The drought affected areas are the 13-month moving average values from the original monthly data. (For interpretation of the references to color in this figure legend, the reader is referred to the web version of this article.)

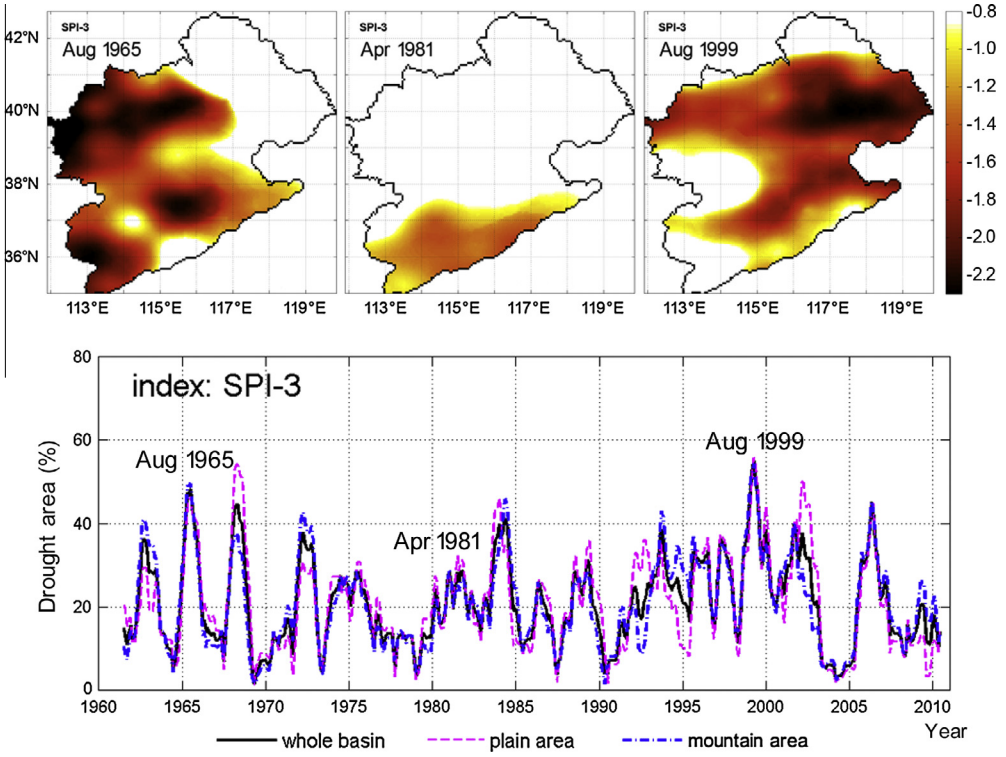

Fig. 7. Spatial patterns of three major droughts and the drought affected areas from 1960 to 2010 derived from the SPI-3. The color bar in upper three maps refers to the drought severity given as SPI-3 value. The drought affected areas are the 13-month moving average values from the original monthly data. (For interpretation of the references to color in this figure legend, the reader is referred to the web version of this article.)

Table 2
List of top fifteen drought events in terms of duration and spatial extent derived from SMDS and SPI.

Index	Event no.	Duration (months)		Total affected area (1000 km^2)	Maximum affected area (1000 km^2)
SMDS	34#	September 2005–March 2008	(31)	315.7	270.9
	30#	August 1998–July 2000	(24)	317.4	242.2
	23#	July 1991–June 1993	(24)	297.9	219.7
	17#	October 1983–August 1985	(23)	313.2	184.1
	14#	July 1980–May 1982	(23)	311.3	243.4
	35#	June 2008–April 2010	(23)	296.7	128.5
	7#	August 1971–January 1973	(18)	249.9	165.0
	10#	April 1975–July 1976	(16)	239.8	91.6
	32#	July 2002–September 2003	(15)	304.8	220.9
	31#	March 2001–May 2002	(15)	280.6	189.8
	18#	April 1986–May 1987	(14)	280.7	168.1
	29#	April 1997–April 1998	(13)	287.6	221.4
	4#	May 1965–May 1966	(13)	287.5	254.9
	19#	July 1987–July 1988	(13)	245.1	92.3
	33#	August 2004–July 2005	(12)	267.7	131.7
SPI	37#	November 2005–February 2007	(16)	315.5	293.0
	17#	April 1981–July 1982	(16)	310.5	198.3
	32#	August 1998–October 1999	(15)	318.8	316.0
	23#	October 1988–December 1989	(15)	316.9	269.6
	12#	December 1974–February 1976	(15)	302.9	203.9
	21#	November 1985–November 1986	(13)	289.4	165.3
	7#	November 1967–October 1968	(12)	318.8	272.4
	5#	January 1965–November 1965	(11)	318.8	250.2
	19#	July 1983–May 1984	(11)	308.5	278.3
	35#	February 2002–November 2002	(10)	300.5	261.4
	28#	September 1994–June 1995	(10)	278.9	214.4
	34#	March 2001–November 2001	(9)	318.1	297.7
	26#	February 1993–October 1993	(9)	291.0	245.5
	38#	June 2007–February 2008	(9)	245.8	138.4
	11#	January 1974–August 1974	(8)	311.5	233.3

Note: 1. The event no. corresponds to the same No. in Fig. 8.
2. The total affected area means the merged monthly affected area in a drought event, and the maximum affected area refers to the largest affected area for a specific drought event.

monthly droughts. Thresholds for drought affected area and duration are given to keep severe drought events only. In this study, large-scale droughts events are defined as initial drought affected areas greater than 20,000 km^2 (or 6.3% of whole basin area) and durations longer than 3 months. Based on these thresholds, a total number of 36 severe drought events were derived from SMDS and 41 events from SPI. Table 2 lists the top 15 severest drought events ranked by the duration and spatial extent, based on the two drought indices. In this table, total affected area means the merged monthly affected area in a drought event, and the maximum affected area refers to the largest affected area in a specific drought event.

The durations and total affected areas of the identified drought events are shown in Fig. 8, in the order of their occurring date. As for drought events derived from SMDS, both the duration and its total affected area are increasing in the past 51 years. The longest duration was from September 2005 to March 2008 (31 months in total, event 34# in Fig. 8a and Table 2). This drought mainly occurred in the northern and central parts and moved southward ending in the spring of 2008, with a total affected area of 315,700 km^2 (covering 99% of the whole basin area). The most areal extensive drought is the event 30#, which occurred from August 1998 to July 2000 (24 months in total) with a total affected area of 317,400 km^2 (nearly covering the whole basin area). In addition, the events occurred in 1965–1966 (event 4#) and 1980–1982 (event 14#) stand out in their respective decade in terms of duration and affected area.

Characteristics of the drought events identified by SPI are illustrated in Fig. 8b. By contrast, these drought events have shorter durations but larger affected areas than those based on SMDS shown in Fig. 8a. The longest duration is only 16 months from November 2005 to February 2007 (event 37#, also see Table 2). As for the spatial extent, average total affected area for the total 41 meteorological drought events is 259,300 km^2 (81% of the basin area), while the average area of 36 agricultural drought events is 209,900 km^2 (66% of the basin area). Moreover, average total affected area of the top-ten extensive meteorological droughts based on SPI is 317,100 km^2, which is also larger than the average total affected area of 301,300 km^2 based on SMDS. The shorter duration of drought events based on SPI can be explained by the interruption of short wet periods (e.g., March–May in 2007). These short wet periods are effective to dampen the meteorological drought severity, but not relatively influential to ease the soil moisture drought. While, the possible explanation for the smaller affected areas of agricultural drought based on SMDS is that this basin has stronger spatial connectivity in hydrology than in meteorology.

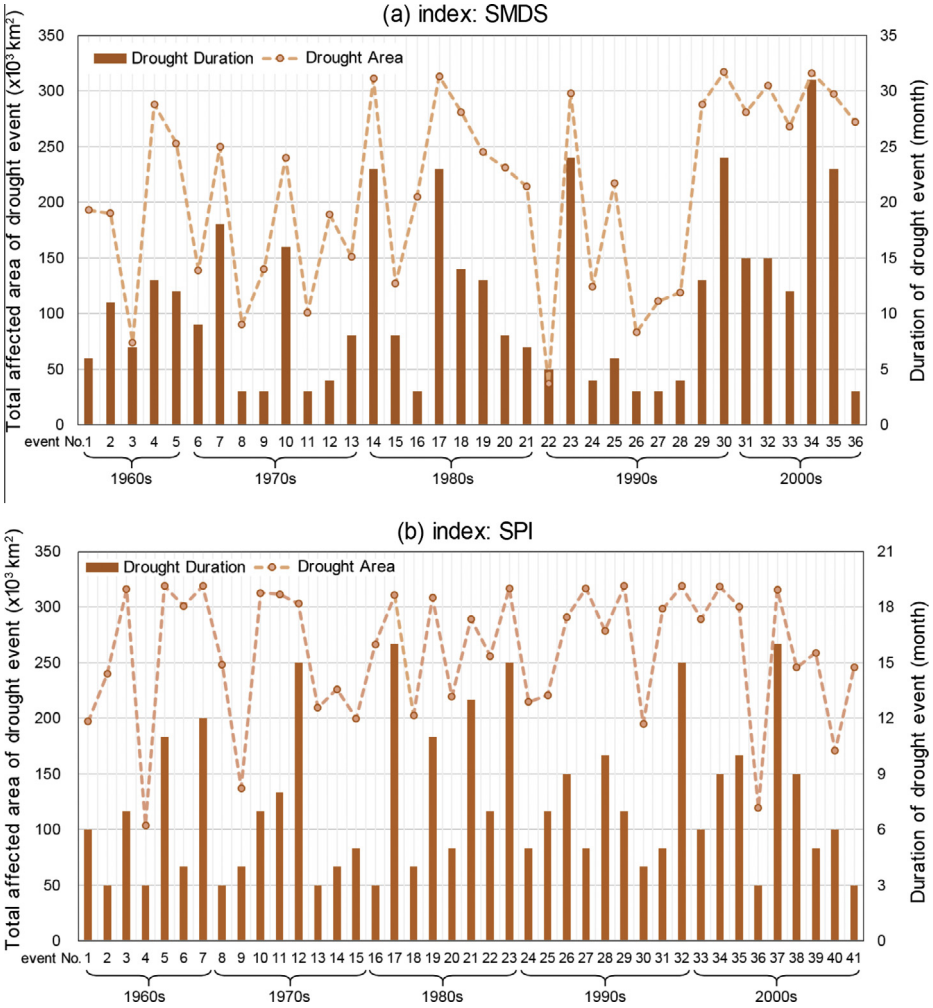

Fig. 8. Duration and total affected area of (a) soil moisture drought events derived from SMDS and (b) meteorological drought events derived from SPI during the period of 1960–2010. The event number is set in the order of drought occurring dates.

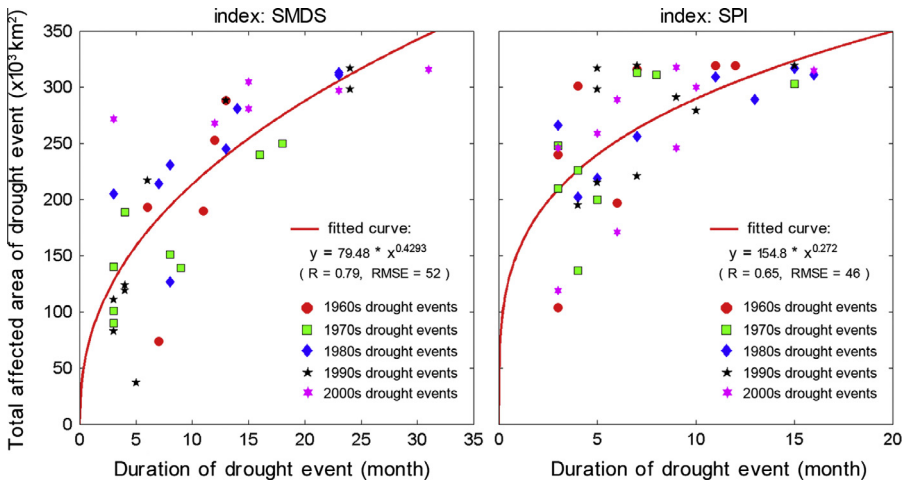

Fig. 9. Duration–area relation curve plotted using all drought events in Haihe basin during the past five decades. The drought events are derived from SMDS and SPI, respectively.

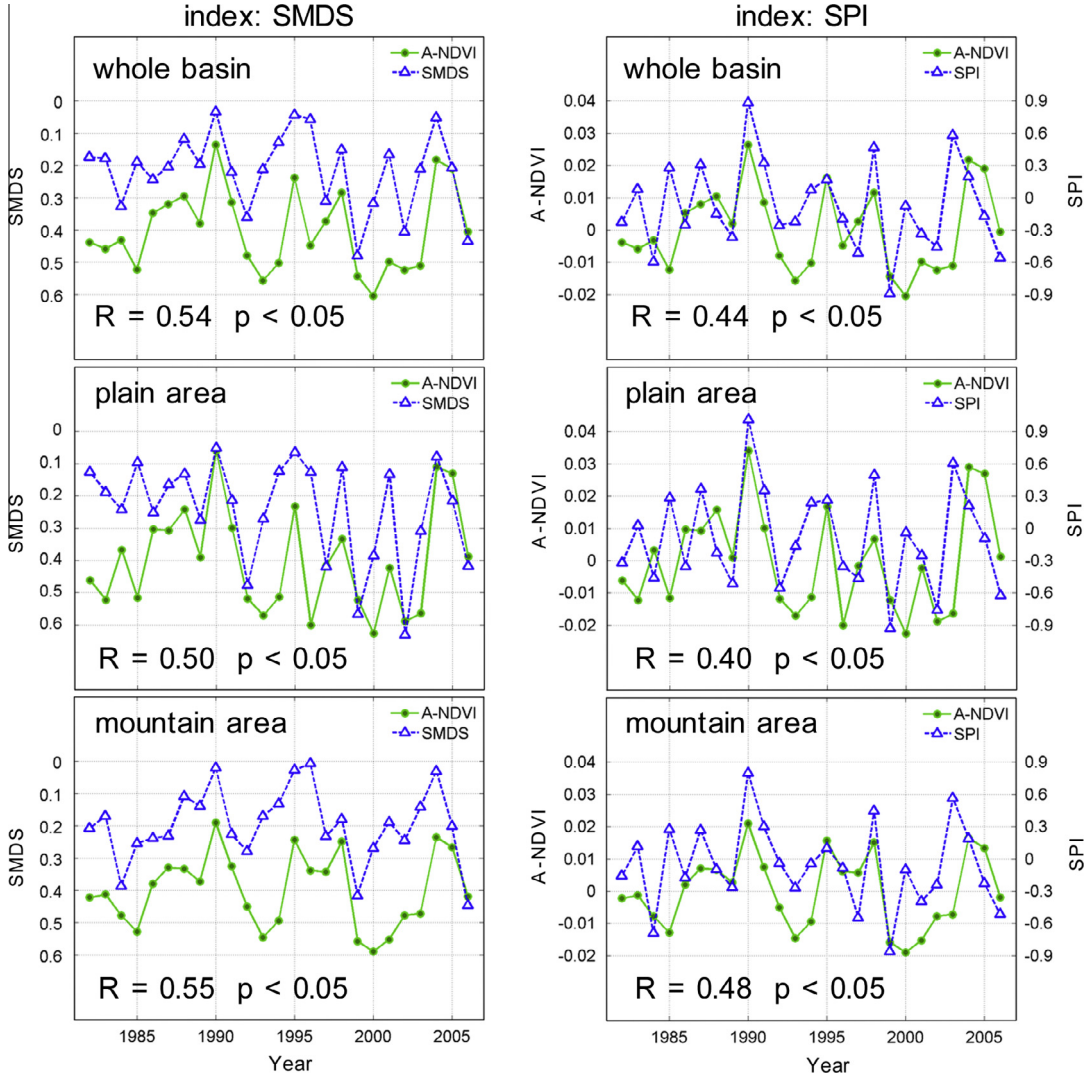

Fig. 10. Interannual variations of SMDS, SPI and A-NDVI in 1982–2006. Correlation between the drought index and A-NDVI and its significance are given in the figure.

5. Discussions

5.1. Relationship between drought duration and affected area

Fig. 9 illustrates the relationship between drought duration and the total affected area. Each spot refers to a drought event derived from SMDS or SPI as plotted in Fig. 8. To identify decadal variation, the drought events are clustered into each decade and represented by different markers. Scatterplot of SMDS shows that drought events in the 1980s, 1990s and 2000s generally have longer durations and larger areas than events in the 1960s and 1970s. In particular, event 34# (September 2005–March 2008) stands out with the largest spatial and temporal extent among all the events. Duration–area relationship is then fitted by the exponential function, with correlation coefficient $R = 0.79$ for SMDS drought events. For the short duration events (3–5 months), the plots show a wide range of total affected area from 37,400 km^2 to 272,000 km^2. When the duration increases (longer than 10 months), spots tend to converge better to the fitted curve, especially for extremely long-term events. As for the SPI scatterplot in Fig. 9, the left and upper bounds on the cloud of points are apparent, which is due to the shorter duration and larger total affected area of the meteorological drought events. Thus, the duration–area relationship fitted by the exponential function has a relatively lower convergence than SMDS, with correlation coefficient $R = 0.65$.

Based on the empirical fitted duration–area function of drought events in the past 51 years, the total affected area of a given drought duration can be approximately estimated. Therefore, the duration–area relation curves in Fig. 9 not only describe relationship between temporal and spatial characteristics of drought events, but also provide an empirical method for the drought impact assessment. This could be a complement to the relationship between drought duration and intensity proposed by the previous study (Sheffield and Wood, 2007).

5.2. Drought impacts on vegetation

As introduced in Section 2.2, annual NDVI of Haihe basin is increasing by 0.01 per decade from 1982 to 2006 (see Fig. 2d). This increasing trend is in agreement with reported conditions by the previous studies in the same region (Zhang et al., 2013; Piao et al., 2010). Under this increasing background, there are two apparent declining periods of NDVI, namely 1992–1994 and 1999–2003, which is consistent with the declining periods of soil moisture as shown in Fig. 3b and with the drought periods in Fig. 5. Furthermore, the droughts occurred in 1992, 1999 and 2002 are among the most remarkable events in the recent 20 years over North China, both in duration and spatial extent (Table 2). As a result the drought impacts on vegetation lasted several years after the drought period ended. In particular, the 1999–2000 drought event is the most severe one in the study period, and it led to the continuously low NDVI for five years from 1999 to 2003 (see Fig. 2d).

We further analyzed the correlation between drought indices and vegetation index to discuss the drought impacts on vegetation. Based on gridded value of each index, regional mean value is calculated as the areal average. The annual average SMDS/SPI is plotted together with A-NDVI, as shown in Fig. 10. The lower index values of SMDS refer to the wet period, while the negative values of SPI or A-NDVI reflect a drought period. Correlation analysis indicates that both of the drought indices are linearly-correlated with the A-NDVI at a significance level of 0.05. Correlation coefficient between the annual areal average SMDS and A-NDVI is 0.54, and is 0.44 between SPI and A-NDVI. Meanwhile, the correlation between NDVI anomaly and drought indices is better for the mountain area than for plain area. Generally, comparison between SMDS and SPI suggests that, in view of drought influence on vegetation, SMDS is a better drought index.

6. Conclusions

Meteorological and soil moisture drought indices were calculated with the continuous precipitation observations and the top 50-cm soil moisture simulated by CLM 4.0 at 0.05° spatial resolution. The temporal and spatial characteristics of droughts in Haihe basin during the past 51 years were analyzed using two probability-based drought indices (i.e., SMDS and SPI). Differences between these two indices were compared and the drought impacts on vegetation were discussed. Based on the results of this study, the following conclusions can be made.

(1) There is a significant increasing trend in drought affected area in Haihe basin over the last five decades, especially after 1980. The drought occurred in the early 2000s is the most extensive and durative one since the 1960s. The plain area with dense population and farmland has suffered more severe droughts in the recent 30 years, and the droughts occurred in 1998, 2000 and 2002 affected larger areas in plain than in mountain area. Droughts derived from SMDS and SPI are generally consistent. But for the droughts occurred in the 1960s, spatial extent derived by SPI is much larger than that by SMDS, which implies that the shortage of precipitation does not certainly cause large-scale drought, because groundwater condition can influence the drought.
(2) Comparative analysis between SMDS and SPI shows that the meteorological drought event generally has shorter duration but larger affected area than the soil moisture drought event, and this can be explained by the difference in spatial connectivity of both meteorology and hydrology in the basin. Based on the identified drought events (36 events by SMDS and 41 events by SPI), it can be concluded that the drought affected area exponentially increases with drought duration, and the fitted exponential function has an acceptable correlation coefficient. This duration–area relation curve can also be used to estimate the potential total affected area for a drought event occurred in this basin.
(3) The annual mean NDVI is increasing since the 1980s in Haihe basin, however, several severe droughts have serious impacts on the vegetation growth, which is indicated by two major declines of NDVI in 1992–1994 and 1999–2003. This is in good agreement with deficit of soil moisture as well as identified drought periods.
(4) The two drought indices (i.e., SMDS and SPI) are compared in view of their relationships with NDVI, and results suggest that the soil-moisture-based drought index (SMDS) is more suitable to reflect actual drought condition of terrestrial ecosystem.

This study used soil moisture of top 50-cm simulated by the land surface model (CLM 4.0) for calculating the drought index SMDS, which may introduce uncertainty to the analysis to some extent. Moreover, human activities on water and land development are not included in model simulation, so the drought situation simulated by the model is more like the natural situation. Besides, drought impacts on vegetation should take into consideration the dynamic vegetation phenology and compare drought index with monthly or seasonal average NDVI. The further study should be carried out in future.

Acknowledgements

The research was supported by the National Natural Science Funds for Distinguished Young Scholar (Project No. 51025931) and National Natural Science Foundation of China (Project No. 51139002).

References

Andreadis, K.M., Clark, E.A., Wood, A.W., Hamlet, A.F., Lettenmaier, D.P., 2005. Twentieth-century drought in the conterminous United States. J. Hydrometeorol. 6 (6), 985–1001.

Anyamba, A., Tucker, C.J., Eastman, J.R., 2001. NDVI anomaly patterns over Africa during the 1997/98 ENSO warm event. Int. J. Remote Sens. 22 (10), 1847–1859.

Bao, Z., Zhang, J., Wang, G., Fu, G., He, R., Yan, X., Jin, J., Liu, Y., Zhang, A., 2012. Attribution for decreasing streamflow of the Haihe River basin, northern China: climate variability or human activities? J. Hydrol. 460, 117–129.

Bryant, E., 2005. Natural Hazards. Cambridge University Press, Cambridge, UK.

China Meteorological Administration (CMA), 1993. Agrometeorological Observation Specification – Soil Volume. China Meteorological Press, Beijing (in Chinese).

China Meteorological Administration (CMA), 2007. Atlas of China Disastrous Weather and Climate. China Meteorological Press, Beijing (in Chinese).

Climate Prediction Center (CPC), 2005. U.S. Soil Moisture Monitoring. National Weather Service.

Dracup, J.A., Lee, K.S., Paulson, E.G., 1980. On the definition of droughts. Water Resour. Res. 16 (2), 297–302.

Federal Emergency Management Agency, 1995. National Mitigation Strategy: Partnerships for Building Safer Communities. FEMA Mitigation Directorate, pp. 40.

Fischer, T., Gemmer, M., Liu, L., Su, B., 2011. Temperature and precipitation trends and dryness/wetness pattern in the Zhujiang River Basin, South China, 1961–2007. Quatern. Int. 244 (2), 138–148.

Food and Agricultural Organization of United Nations (FAO), 2002. Report of FAO-CRIDA Expert Group Consultation on Farming System and Best Practices for Drought-prone Areas of Asia and the Pacific Region. Central Research Institute for Dryland Agriculture, Hyderabad.

Fu, C., An, Z., 2002. Study of aridification in northern China – a global change issue facing directly the demand of nation. Earth Sci. Front. 9 (2), 271–275 (in Chinese).

Gocic, M., Trajkovic, S., 2013. Analysis of precipitation and drought data in Serbia over the period 1980–2010. J. Hydrol. 494, 32–42.

Guttman, N.B., 1998. Comparing the Palmer drought index and the Standardized Precipitation Index. J. Am. Water Resour. As. 34 (1), 113–121.

Guttman, N.B., 1999. Accepting the Standardized Precipitation Index: a calculation algorithm. J. Am. Water Resour. As. 35 (2), 311–322.

Haihe River Commission, 2004a. <http://www.hwcc.gov.cn/pub/hwcc/static/lygk/qxsw.htm>.

Haihe River Commission, 2004b. <http://www.hwcc.gov.cn/pub/hwcc/static/lygk/shzh.htm>.

Haihe River Commission, 2012. <http://www.hwcc.gov.cn/pub2011/hwcc/wwgj/haiweiyw/201203/t20120321_341780.htm>.

Hao, Z., AghaKouchak, A., 2013. Multivariate Standardized Drought Index: a parametric multi-index model. Adv. Water Resour. 57, 12–18.

Hou, Z., Huang, M., Leung, L.R., Lin, G., Ricciuto, D.M., 2012. Sensitivity of surface flux simulations to hydrologic parameters based on an uncertainty quantification framework applied to the Community Land Model. J. Geophys. Res. 117 (D15108).

Huang, M., Hou, Z., Leung, L.R., Ke, Y., Liu, Y., Fang, Z., Sun, Y., 2013. Uncertainty analysis of runoff simulations and parameter identifiability in the Community Land Model: evidence from MOPEX basins. J. Hydrometeorol. 14 (6), 1754–1772.

Kendall, M., 1975. Rank Correlation Methods, 4th ed. Charles Griffin, p. 202.

Lawrence, D.M., Oleson, K.W., Flanner, M.G., Thornton, P.E., Swenson, S.C., Lawrence, P.J., Zeng, X., Yang, Z., Levis, S., Sakaguchi, K., Bonan, G.B., Slater, A.G., 2011. Parameterization improvements and functional and structural advances in version 4 of the Community Land Model. J. Adv. Modell. Earth Syst. 3 (M03001).

Lei, H., Yang, D., Cai, J., Wang, F., 2013. Long-term variability of the carbon balance in a large irrigated area along the lower Yellow River from 1984 to 2006. Sci. China-Earth Sci. 56 (4), 671–683.

Lei, H., Yang, D., Huang, M., 2014. Impacts of climate change and vegetation dynamics on runoff in the mountainous region of the Haihe River basin in the past five decades. J. Hydrol. 511, 786–799.

Li, W., Qin, Z., Lin, L., 2010. Quantitative analysis of agro-drought impact on food security in China. J. Nat. Disasters 19 (3), 111–118 (in Chinese).

Li, H., Huang, M., Wigmosta, M.S., Ke, Y., Coleman, A.M., Leung, L.R., Wang, A., Ricciuto, D.M., 2011a. Evaluating runoff simulations from the Community Land Model 4.0 using observations from flux towers and a mountainous watershed. J. Geophys. Res. 116 (D24120).

Li, Q., Nakatsuka, T., Kawamura, K., Liu, Y., Song, H., 2011b. Hydroclimate variability in the North China plain and its link with El nino-southern oscillation since 1784 AD: insights from tree-ring cellulose delta O-18. J. Geophys. Res. 116 (D22106).

Liu, J.Y., Liu, M.L., Tian, H.Q., Zhuang, D.F., Zhang, Z.X., Zhang, W., Tang, X.M., Deng, X.Z., 2005. Spatial and temporal patterns of China's cropland during 1990–2000: an analysis based on landsat TM data. Remote Sens. Environ. 98 (4), 442–456.

Liu, K., Wang, W., Zhu, Y., Wang, H., 2012. Trend of drought and its relationship with extreme precipitation in Huaihe River basin over the last 60 years. J. Hydraul. Eng. 43 (10), 1179–1187 (in Chinese).

Long, D., Scanlon, B.R., Longuevergne, L., Sun, A.Y., Fernando, D.N., Save, H., 2013. GRACE satellite monitoring of large depletion in water storage in response to the 2011 drought in Texas. Geophys. Res. Lett. 40 (13), 3395–3401.

Lu, L., Liu, J., Qin, D., 2011. Analysis of drought/waterlogging variation tendency and evolution features in Haihe River Basin during 1469–2008 years. Water Res. Power 29 (9), 8–11 (in Chinese).

Mann, H.B., 1945. Nonparametric test against trend. Econometrica 13 (3), 245–259.

McKee, T.B., Doesken, N.J., Kleist, J., 1993. The relationship of drought frequency and duration to time scales. In: Paper Presented at 8th Conference on Applied Climatology. American Meteorological Society, Anaheim, CA, pp. 179–183.

McKee, T.B., Doesken, N.J., Kleist, J., 1995. Drought monitoring with multiple time scales. In: Paper Presented at 9th Conference on Applied Climatology. American Meteorological Society, Dallas, TX, pp. 233–236.

Mishra, A.K., Singh, V.P., 2010. A review of drought concepts. J. Hydrol. 391 (1), 202–216.

Mishra, A.K., Singh, V.P., 2011. Drought modeling – a review. J. Hydrol. 403 (1), 157–175.

Moran, M.S., Clarke, T.R., Inoue, Y., Vidal, A., 1994. Estimating crop water deficit using the relation between surface–air temperature and spectral vegetation index. Remote Sens. Environ. 49 (3), 246–263.

National Climatic Data Center, 2003. Coop summary of the day-CDMP-Pre, Data documentation for data set 3206 (DSI-3206), pp. 18.

Oleson, K.W., Lawrence, D.M., Bonan, G.B., Flanner, M.G., Kluzek, E., Lawrence, P.J., Levis, S., Swenson, S.C., Thornton, P.E., Dai, A., Decker, M., Dickinson, R., Feddema, J., Heald, C.L., Hoffman, F., Lamarque, J.-F., Mahowald, N., Niu, G.-Y., Qian, T., Randerson, J., Running, S., Sakaguchi, K., Slater, A., Stockli, R., Wang, A., Yang, Z.-L., Zeng, Xi, Zeng, Xu, 2010. Technical Description of Version 4.0 of the Community Land Model (CLM). NCAR Technical Note NCAR/TN-478+STR, National Center for Atmospheric Research, Boulder, CO, 257 pp.

Palmer, W.C., 1968. Keeping track of crop moisture conditions, nationwide: the new crop moisture index. Weatherwise 21, 156–161.

Piao, S., Ciais, P., Huang, Y., Shen, Z., Peng, S., Li, J., Zhou, L., Liu, H., Ma, Y., Ding, Y., Friedlingstein, P., Liu, C., Tan, K., Yu, Y., Zhang, T., Fang, J., 2010. The impacts of climate change on water resources and agriculture in China. Nature 467 (7311), 43–51.

Shangguan, W., Dai, Y., Liu, B., Ye, A., Yuan, H., 2012. A soil particle-size distribution dataset for regional land and climate modelling in China. Geoderma 171 (SI), 85–91.

Sheffield, J., Wood, E.F., 2007. Characteristics of global and regional drought, 1950-2000: Analysis of soil moisture data from off-line simulation of the terrestrial hydrologic cycle. J. Geophys. Res. 112 (D17115D17).

Sheffield, J., Wood, E.F., 2008. Global trends and variability in soil moisture and drought characteristics, 1950–2000, from observation–driven simulations of the terrestrial hydrologic cycle. J. Climate 21 (3), 432–458.

Sheffield, J., Andreadis, K.M., Wood, E.F., Lettenmaier, D.P., 2009. Global and continental drought in the second half of the twentieth century: severity–area–duration analysis and temporal variability of large-scale events. J. Climate 22 (8), 1962–1981.

Shi, X., Mao, J., Thornton, P.E., Huang, M., 2013. Spatiotemporal patterns of evapotranspiration in response to multiple environmental factors simulated by the Community Land Model. Environ. Res. Lett. 8 (0240122).

Stöckli, R., Lawrence, D.M., Niu, G.Y., Oleson, K.W., Thornton, P.E., Yang, Z.L., Bonan, G.B., Denning, A.S., Running, S.W., 2008. Use of FLUXNET in the community land model development. J. Geophys. Res. 113 (G01025G1).

Thomas, A.C., Reager, J.T., Famiglietti, J.S., Rodell, M., 2014. A GRACE-based water storage deficit approach for hydrological drought characterization. Geophys. Res. Lett. 41 (5), 1537–1545.

U.S. Drought Monitor, 2003. Drought Monitor: State-of-the-Art Blend of Science and Subjectivity. National Drought Mitigation Center.

Wang, A., Zeng, X., 2011. Sensitivities of terrestrial water cycle simulations to the variations of precipitation and air temperature in China. J. Geophys. Res. 116 (D02107).

Wang, A., Lettenmaier, D.P., Sheffield, J., 2011. Soil moisture drought in China, 1950–2006. J. Climate 24 (13), 3257–3271.

World Meteorological Organization (WMO), 1986. Report on Drought and Countries Affected by Drought During 1974–1985, Geneva.

World Meteorological Organization (WMO), 2012. Standardized Precipitation Index User Guide (WMO-No.1090), Geneva.

Xu, X., Yang, D., Yang, H., Lei, H., 2014. Attribution analysis based on the Budyko hypothesis for detecting the dominant cause of runoff decline in Haihe basin. J. Hydrol. 510, 530–540.

Yang, D.W., Li, C., Hu, H.P., Lei, Z.D., Yang, S.X., Kusuda, T., Koike, T., Musiake, K., 2004. Analysis of water resources variability in the Yellow River of China during the last half century using historical data. Water Resour. Res. 40 (W065026).

Yevjevich, V., 1967. An Objective Approach to Definitions and Investigations of Continental Hydrologic Droughts. Colorado State University, Fort Collins, Colo.

Yuan, W., Zhou, G., 2004. Comparison between standardized precipitation index and Z-index in China. Acta Phytoecol. Sin. 28 (4), 523–529 (in Chinese).

Zhai, J., Liu, B., Hartmann, H., Su, B., Jiang, T., Fraedrich, K., 2010a. Dryness/wetness variations in ten large river basins of China during the first 50 years of the 21st century. Quatern. Int. 226 (1–2), 101–111.
Zhai, J., Su, B., Krysanova, V., Vetter, T., Gao, C., Jiang, T., 2010b. Spatial variation and trends in PDSI and SPI indices and their relation to streamflow in 10 large regions of China. J. Climate 23 (3), 649–663.
Zhang, Q., Xu, C., Zhang, Z., 2009. Observed changes of drought/wetness episodes in the Pearl River basin, China, using the standardized precipitation index and aridity index. Theor. Appl. Climatol. 98 (1–2), 89–99.
Zhang, X., Dai, J., Ge, Q., 2013. Variation in vegetation greenness in spring across eastern China during 1982–2006. J. Geogr. Sci. 23 (1), 45–56.
Zhao, G., Mu, X., Hoermann, G., Fohrer, N., Xiong, M., Su, B., Li, X., 2012. Spatial patterns and temporal variability of dryness/wetness in the Yangtze River Basin, China. Quatern. Int. 282, 5–13.